Journal of Food Engineering 130 (2014) 23–35

Contents lists available at ScienceDirect

Journal of Food Engineering

journal homepage: www.elsevier.com/locate/jfoodeng

Modelling heat and mass transfer in deformable porous media: Application to bread baking

V. Nicolas [a,b], P. Salagnac [b], P. Glouannec [a,*], J.-P. Ploteau [a], V. Jury [c], L. Boillereaux [c]

[a] Laboratoire d'Ingénierie des MATériaux de Bretagne – Equipe Thermique et Energétique, Université Européenne de Bretagne, B.P. 92116, 56321 Lorient Cedex, France
[b] Laboratoire des Sciences de l'Ingénieur pour l'Environnement, Université de La Rochelle, Pôle Sciences et Technologie, Av. M. Crépeau, 17042 La Rochelle Cedex 1, France
[c] Laboratoire de Génie des Procédés, Environnement, Agroalimentaire, ONIRIS, Rue de la Géraudière, B.P. 82225, 44322 Nantes Cedex 3, France

ARTICLE INFO

Article history:
Received 26 July 2013
Received in revised form 15 January 2014
Accepted 21 January 2014
Available online 2 February 2014

Keywords:
Porous media
Deformation
Heat and mass transfer
Simulation
Bread baking

ABSTRACT

Bread passes through different states during baking: the dough turns into crumb and then into crust, heat and mass transfers cause different phenomena to occur inside the product (mass loss, temperature increase, CO_2 production, gelatinization, swelling, etc.). This study is devoted to "French baguette" contact baking. The product is subjected to heat by conduction, natural convection and infrared radiation.

A numerical model was developed using the finite element method. This model allows predicting evolutions of temperature, water content, gas pressure and deformation. Local porosity and gas fraction are also calculated.

An experimental approach was implemented in order to compare numerical results and experimental evolutions (temperature and mass loss). Experimental boundary conditions were used for the simulations while the properties of the product were taken from the literature.

Sensitivity studies of the mechanical properties, model parameters, and water activity parameters were performed.

1. Introduction

With 4 million tons of bread produced annually, bakery is the leading craft sector in France. Artisanal bread (with about 30,000 craft-bakers) still represents 61% of total production, although the proportion of industrial bread has been rising steadily for a decade. Certain previous studies have emphasized that considerable energy is required to make bread: 5 MJ/kg bread, which is high in comparison to other thermal operations. This considerable energy is mainly consumed for crust development, due to the high vaporisation heat required at this step. Therefore, in order to control this energy, it is necessary to determine the thermal behaviour of the processes involved during bread baking.

Bread is a complex medium in which many coupled physical phenomena occur during baking, like heat and mass transfers, the evaporation of water, volume expansion, starch gelatinization, the formation of the porous structure, crust formation, and surface browning reaction.

The product is composed of 100 g flour, 60 g water, 3 g yeast and 2.2 g salt (Jury et al., 2007; Mondal and Datta, 2008). Other ingredients can be added to change the properties of the dough (Stampfli and Nersten, 1995). First, the ingredients are mixed after which the dough is placed in a controlled atmosphere to ensure its porosity. Finally, after scarification, the expanded dough is placed in the oven to be baked.

The first phenomenon to occur during baking is the formation of carbon dioxide bubbles (Chiotellis and Campbell, 2003a, b). Initially the bubbles are isolated from each other, without the transfer of gas. Yeast fermentation releases carbon dioxide that causes porosity to increase (Bellido et al., 2009, 2008), leading to increased pressure. The fermentation rate increases by 8% for each additional degree, starting from 20 °C up to 40 °C. From 40 °C, this activity decreases and then stops at 50 °C. Rheological properties have a significant effect on deformation and gelatinization occurs at about 60 °C when the dough turns into crumbs (Rouillé et al., 2010). Deformation is constrained as the solid structure of the crust starts to form. The last phenomenon that occurs during baking is browning.

The water content stays at its initial value in the dough and crumb throughout the baking process (Wagner et al., 2007). The temperature in the crumb rises to 100 °C, i.e. water vaporisation temperature. When the temperature exceeds 100 °C, the crumb dries, the temperature increases and the crust is formed (Mondal and Datta, 2008).

* Corresponding author. Tel.: +33 02 97 87 45 11; fax: +33 02 97 87 45 00.
E-mail address: Patrick.Glouannec@univ-ubs.fr (P. Glouannec).

http://dx.doi.org/10.1016/j.jfoodeng.2014.01.014
0260-8774/

Nomenclature

a_w	water activity
C_p	specific heat (J kg^{-1} K^{-1})
D	mass diffusivity (kg m^{-1} s^{-1})
fc	crust function
F_m	surface mass flux (kg m^{-2} s^{-1})
G	irradiation (W m^{-2})
h_c	convective heat transfer coefficient (W m^{-2} K^{-1})
k	permeability (m s^{-1})
k_m	convective mass transfer coefficient (m s^{-1})
K	phase change rate (kg m^{-3} s^{-1})
Le	Lewis number
L_v	latent heat (J kg^{-1})
n	mass flux (kg s^{-1})
Nu	Nusselt number
M	molar mass
m	mass (kg)
P	pressure (Pa)
Pr	Prandtl number
R	universal gas constant (J K^{-1} mol^{-1})
Ra	Rayleigh number
R_c	thermal contact resistance (K m^2 W^{-1})
R_{CO_2}	carbon dioxide generation (kg_{CO2} $kg^{-1}_{\text{dry matter}}$ s^{-1})
S	saturation
T	temperature (K or °C)
t	time (s)
V	Volume (m^3)
$\vec{V}$	velocity (m s^{-1})
W	moisture content (kg kg^{-1})

Greek symbols

ε	porosity, volume fraction (m^3 m^{-3})
ε_m	infrared emissivity
λ	thermal conductivity (W m^{-1} K^{-1})
μ	dynamic viscosity (kg m^{-1} s^{-1})
ρ	density (kg m^{-3})
σ	Stephan-Boltzmann constant (W m^{-2} K^{-4}); stress (Pa)

Subscripts

0	initial
a	air
atm	atmospheric
CO_2	carbon dioxide
D	diameter
eff	effective
g	gas
inf	infinite
l	liquid water
rl	liquid relative
s	solid
hearth	hearth
surf	surface
v	water vapour

Superscripts

a	apparent
eff	effective
i	intrinsic

Coupling all these phenomena is complex because they are interdependent. Different mathematical models can be found in the scientific literature to study the mass and thermal evolutions of bread during baking. They can be classified into two categories:

- Diffusive models (Purlis and Salvadori, 2009a, b; Thorvaldsson and Janestad, 1999; Tong and Lund, 1993; Zanoni et al., 1994). In these models, only temperature and moisture content are calculated. The liquid and vapour phases are not separated, but an equivalent global diffusion coefficient is used. The deformation of the bread is only calculated with experimental correlations (Purlis and Salvadori, 2010).
- Multiphasic models (Lostie et al., 2004, 2002; Ousegui et al., 2010; Zhang and Datta, 2006; Zhang et al., 2005). For these models, the mass conservation equations are written for each phase. The mass diffusion coefficient is not apparent but is calculated for each phase. In addition to temperature and moisture content, these models introduce gas pressure and deformation.

It may also be noted that one model uses the Lattice-Boltzmann method (Hussein and Becker, 2010).

In this article a numerical knowledge model is developed to simulate the baking of a French "baguette" by direct conduction, infrared radiation and natural convection. This model takes into account the major physical phenomena occurring during baking:

- A complete heat and mass transfer system of equations for deformable porous media, with the conservation equation of apparent solid density to calculate local porosity.
- Deformation with Terzaghi effective stress; and different boundary conditions.
- Convective and radiative heat transfers at the air/bread interface.
- Thermal conduction at the hearth/bread interface.

First, the assumptions of the physical model are explained. Then, we present the equations of conservation of mass and energy and the boundary conditions. The properties used in the model are described and the numerical model is presented. Next, a sensitivity study of the mesh is performed after which simulations are compared with experimental data. Lastly, a sensitivity study is performed on water activity and mechanical properties.

2. Physical model

In this study, the bread is heated by direct conduction from the hearth, natural convection and infrared radiation (Fig. 1).

The medium studied consists of three phases: solid (s), liquid (l) and gas (g). The liquid phase is water. The gaseous phase consists of a perfect blend of gas: carbon dioxide (CO_2) and vapour (v) (Fan et al., 1999). The air phase is assumed to be included in the carbon dioxide phase.

$$\rho_g^i = \frac{P_i M_i}{RT} \quad \text{for } i = (v, CO_2) \quad \text{with} \quad P_g = P_v + P_{CO_2} \quad \text{and}$$
$$\rho_g^i = \rho_v^i + \rho_{CO_2}^i$$

Furthermore, local thermodynamic equilibrium is assumed beforehand while thermal radiation within the material and gravity are neglected.

The model developed is based on the equations of conservation of mass and heat. It provides access to the local variables, namely moisture content $\left(W = \frac{m_l}{m_s}\right)$, gas pressure P_g, gas volume fraction ε_g and temperature T. In addition, an equation of conservation of momentum is used to evaluate the velocity $\vec{V}$ of the porous matrix.

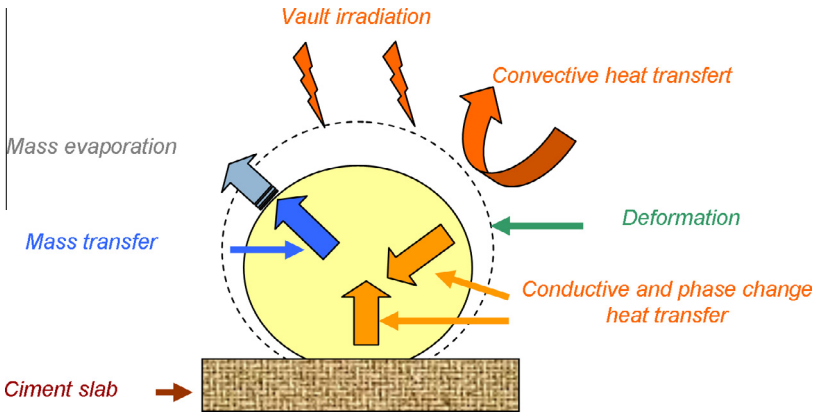

Fig. 1. Diagram of the device and transfers which occurs during baking.

2.1. Governing equations

Four constituents are considered: liquid water (l), water vapour (v), carbon dioxide (CO_2) and solid (s). For each constituent, mass conservation equations are written (Bird et al., 2002). These equations are composed of an inertial term, mass fluxes $\vec{n}$, deformation (Cáceres Salazar, 2006; Zhang and Datta, 2006), and source term K.

$$\frac{\partial \rho_l^a}{\partial t} + \vec{\nabla}\cdot\left(\vec{n}_l + \rho_l^a \vec{V}\right) = -K_v \tag{1}$$

$$\frac{\partial \rho_v^a}{\partial t} + \vec{\nabla}\cdot\left(\vec{n}_v + \rho_v^a \vec{V}\right) = K_v \tag{2}$$

$$\frac{\partial \rho_{CO_2}^a}{\partial t} + \vec{\nabla}\cdot\left(\vec{n}_{CO_2} + \rho_{CO_2}^a \vec{V}\right) = K_{CO_2} \tag{3}$$

$$\frac{\partial \rho_s^a}{\partial t} + \vec{\nabla}\cdot\left(\rho_s^a \vec{V}\right) = 0 \tag{4}$$

The mass fluxes are written as a function of moisture content (W), temperature (T) and gas pressure (P_g).

For the liquid flux, the assumption of Zhang and Datta (2006) that liquid water is strongly bound to starch is applied. Only capillary liquid flux occurs in the dough. A diffusive flux due to the moisture content gradient is used:

$$\vec{n}_l = D_l^W \vec{\nabla} W \tag{5}$$

Gas mass fluxes $\vec{n}_i$ ($i = v, CO_2$) are described by two phenomena. The first is a convective flux which depends on the mean filtration velocity. Convective motions of liquid and gas in unsaturated media are usually described by the generalized Darcy law. This allows using the average velocity of liquid and gaseous phases. The second phenomenon comes from Fick's law. It is a diffusive flux which depends on the mass fraction (Bird et al., 2002). These two fluxes are written as a function of driven gradients (Salagnac et al., 2004):

$$\begin{aligned}\vec{n}_v &= -\rho_v^i \frac{k_{in} k_{rg}}{\mu_g}\vec{\nabla} P_g - \rho_g^i D_v^{eff}\vec{\nabla}\omega_v \\ &= D_v^W \vec{\nabla} W + D_v^T \vec{\nabla} T + D_v^{P_g}\vec{\nabla} P_g\end{aligned} \tag{6}$$

$$\begin{aligned}\vec{n}_{CO_2} &= -\rho_{CO_2}^i \frac{k_{in} k_{rg}}{\mu_g}\vec{\nabla} P_g - \rho_g^i D_v^{eff}\vec{\nabla}\omega_{CO_2} \\ &= D_{CO_2}^W \vec{\nabla} W + D_{CO_2}^T \vec{\nabla} T + D_{CO_2}^{P_g}\vec{\nabla} P_g\end{aligned} \tag{7}$$

2.2. System of equations

2.2.1. Moisture content equation

Water content is defined by the ratio between the mass of liquid water and the dry mass. The moisture content equation is obtained from liquid and water vapour mass conservation:

$$\frac{\partial \rho_l^a}{\partial t} = \zeta_1 \frac{\partial W}{\partial t} - \zeta_2 \frac{\partial \varepsilon_g}{\partial t} \quad \text{and} \quad \frac{\partial \rho_v^a}{\partial t} = \beta_1 \frac{\partial T}{\partial t} + \beta_2 \frac{\partial W}{\partial t} + \beta_3 \frac{\partial \varepsilon_g}{\partial t} \tag{8}$$

$$\begin{aligned}&(\zeta_1 + \beta_2)\frac{\partial W}{\partial t} + \vec{\nabla}\cdot\begin{pmatrix}\left(D_l^W + D_v^W\right)\vec{\nabla} W + D_v^T \vec{\nabla} T + D_v^{P_g}\vec{\nabla} P_g \\ \left(\rho_l^a + \rho_v^a\right)\vec{V}\end{pmatrix} \\ &\quad = -\beta_1 \frac{\partial T}{\partial t} - (\beta_3 - \zeta_2)\frac{\partial \varepsilon_g}{\partial t}\end{aligned} \tag{9}$$

The different terms of these equations are explained in Appendices B and C.

2.2.2. Gas pressure equation

The equation of the total pressure of the gaseous phase P_g is obtained from the mass conservation equation of carbon dioxide (Salagnac et al., 2004). This equation is derived from a change of state variable from $\rho_{CO_2}^a$ to P_g.

$$\begin{aligned}\frac{\partial P_g}{\partial t} = \frac{1}{\gamma_3}\Big[&\vec{\nabla}\cdot\left(D_{CO_2}^W \vec{\nabla} W + D_{CO_2}^T \vec{\nabla} T + D_{CO_2}^{P_g}\vec{\nabla} P_g + D_{CO_2}^g \vec{g} + \rho_{CO_2}^a \vec{V}\right) \\ &-\gamma_1 \frac{\partial T}{\partial t} - \gamma_2 \frac{\partial W}{\partial t} - \gamma_4 \frac{\partial \varepsilon_g}{\partial t} + K_{CO_2}\Big]\end{aligned} \tag{10}$$

2.2.3. Gas fraction equation

The local gas fraction equation is calculated from the solid conservation equation.

$$\left(\frac{\rho_s^i}{\rho_l^i}\zeta_2 - \rho_s^i\right)\frac{\partial \varepsilon_g}{\partial t} + \vec{\nabla}\cdot\left(\rho_s^a \vec{V}\right) = \frac{\rho_s^i}{\rho_l^i}\zeta_1 \frac{\partial W}{\partial t} \tag{11}$$

The gas fraction allows calculating the porosity as a function of solid matrix deformation and water content. In this article porosity is defined by the fraction of the "liquid + gas" volume of the total volume:

$$\varepsilon = \frac{\varepsilon_g + \frac{\rho_s^i W}{\rho_l^i}}{1 + \frac{\rho_s^i W}{\rho_l^i}} \tag{12}$$

2.2.4. Energy equation

The phenomena taken into account are the displacement of porous matrix, conduction, convection and phase change (evaporation–condensation).

$$\rho c_p \frac{\partial T}{\partial t} + \begin{bmatrix} \left(\vec{n}_l + \rho_l^a \vec{V}\right) c_{p,l} \vec{\nabla} T + \left(\rho_s^a \vec{V}\right) c_{p,s} \vec{\nabla} T \\ + \left(\vec{n}_v + \rho_v^a \vec{V}\right) c_{p,v} \vec{\nabla} T + \left(\vec{n}_{CO_2} + \rho_{CO_2}^a \vec{V}\right) c_{p,CO_2} \vec{\nabla} T \end{bmatrix} = \vec{\nabla} \cdot \left(\lambda \vec{\nabla} T\right) - K_v L_v \quad (13)$$

The phase change rate is deduced from the liquid water conservation equation.

$$K_v = -\left(\zeta_1 \frac{\partial W}{\partial t} - \zeta_2 \frac{\partial \varepsilon_g}{\partial t} + \vec{\nabla} \cdot \left(D_l^W \vec{\nabla} W + \rho_l^a \vec{V}\right)\right) \quad (14)$$

2.2.5. Deformation

A viscoelastic model is used with a Terzaghi effective stress (Bishop, 1960; Chemkhi and Zagrouba, 2008; Dhall and Datta, 2011). Variable elastic modulus E and time relaxation as a function of the product state are employed, i.e. dough, crumb and crust. This equation expresses the mechanical equilibrium between the product and gas pressure. Gas pressure is the driving force of the swelling.

$$\vec{\nabla} \cdot \left(\bar{\bar{\sigma}}_{\text{eff}}\right) = \vec{\nabla} P_g \quad (15)$$

2.3. Boundary conditions

2.3.1. Air/product interface

Fig. 1 shows all the transfer mechanisms occurring at the interface with the air. The bread is heated by convection and infrared radiation while water evaporation occurs at the surface.

2.3.1.1. Moisture content equation. Water evaporation occurs on the surface of the bread. The evaporation mass flow *Fm* depends on the difference of partial vapour pressure between the bread surface and the hot air (Incropera and DeWitt, 2002):

$$-\vec{n} \cdot \left(\vec{n}_l + \vec{n}_v\right) = F_m \quad (16)$$

$$F_m = \frac{k_m M_v}{R} \left(\frac{P_{v,\text{surf}}}{T} - \frac{P_{v,\text{inf}}}{T_a}\right) \quad (17)$$

The mass transfer k_m coefficient is estimated from the convective heat transfer coefficient with the Colburn analogy (Incropera and DeWitt, 2002)

$$k_m = \frac{h_c}{\rho c_p \text{Le}^{2/3}} \quad (18)$$

2.3.1.2. Gas pressure equation. The total gas pressure is assumed to be constant and equal to atmospheric pressure. A Dirichlet condition is applied.

$$P_g = P_{\text{atm}} \quad (19)$$

2.3.1.3. Gas fraction equation. The velocity calculated at the surface by the equation of deformation is imposed.

$$-\vec{n} \cdot \left(\rho_s^a \vec{V}\right) = \vec{n} \cdot \left(\rho_s^a \vec{V}_{\text{surf}}\right) \quad (20)$$

2.3.1.4. Energy equation. Two types of heat exchange coexist at the interface between the air and the product: convection and radiation. For infrared radiation, surfaces are treated as grey bodies. A radiative flux *G* is imposed.

$$-\vec{n} \cdot \left(\lambda \vec{\nabla} T + \vec{n}_l L_v\right) = h_c (T_a - T) + \varepsilon_m \left[G - \sigma T^4\right] \quad (21)$$

For the convection coefficient h_c a correlation corresponding to natural convection around a horizontal cylinder is used (Incropera and DeWitt, 2002).

$$\text{Nu} = \left[0.6 + \frac{0.387 Ra_D^{1/6}}{\left[1 + (0.559/\text{Pr})^{9/16}\right]^{8/27}}\right]^2 \quad (22)$$

2.3.2. Hearth/product interface

The evaluation of the hearth temperature T_{hearth} is obtained by solving the heat equation:

$$\rho_{\text{hearth}} C_{p,\text{hearth}} \frac{\partial T_{\text{hearth}}}{\partial t} = \vec{\nabla} \cdot \left(\lambda_{\text{hearth}} \vec{\nabla} T_{\text{hearth}}\right) \quad (23)$$

The temperature is imposed for the lower face of the hearth and exchange by convection is assumed for the upper surface without bread (Fig. 2).

The heat flux exchanged with bread is then expressed by the following expression:

$$\phi_{\text{hearth}} = \frac{T_{\text{hearth}} - T}{R_c} \quad (24)$$

where R_c is a thermal contact resistance. In this work a constant value is taken after numerical adjustment.

At the hearth/product interface, a zero mass flux is imposed:

$$-\vec{n} \cdot \left(\vec{n}_l + \vec{n}_v\right) = 0 \quad (25)$$

A velocity of zero is imposed for deformation.

2.4. Physical properties

2.4.1. Water activity

Two models are used in this work. The first is the Oswin model adjusted by Jury (Jury, 2007) based on experimental evolutions.

$$100W = A\left(\frac{a_w}{1 - a_w}\right)^B \quad (26)$$

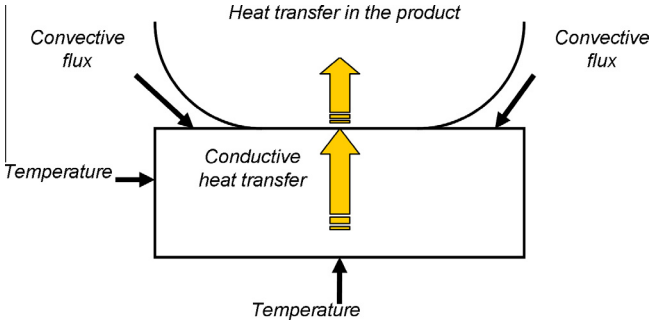

Fig. 2. Heat transfer from hearth to bread.

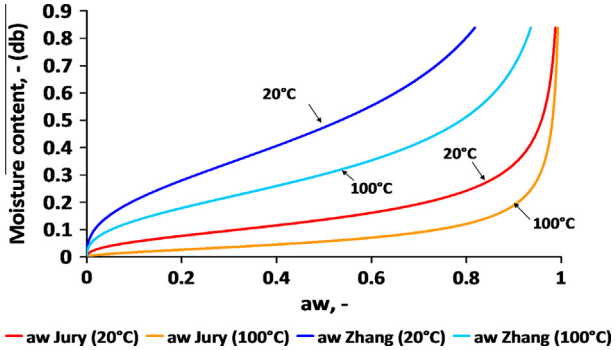

Fig. 3. Desorption isotherms as function of moisture content and temperature.

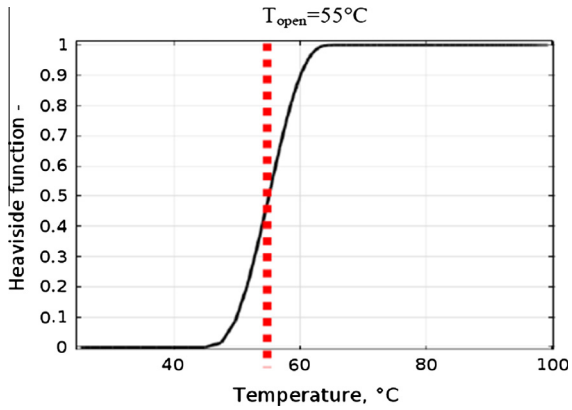

Fig. 4. Pore opening function.

Table 1
Properties used in the model.

Pore opening function range, ΔT	10	°C
Solid intrinsic density, ρ_s^i	1500	kg m^{-3}
Solid heat capacity, $c_{p,s}$	1440	J kg^{-1} K^{-1}
Solid conductivity, λ_s	0.7	W m^{-1} K^{-1}
Infrared emissivity, ε_m	0.9	–

The second is a fitted model used in the literature (Zhang et al., 2005; Zhang and Datta, 2006; Purlis and Salvadori, 2009a,b; Ousegui et al., 2010). The evolution of Zhang's desorption isotherm is higher than that of Jury (Fig. 3). These two evolutions are temperature dependent (with coefficients A and B for Jury's model).

2.4.2. Liquid diffusion coefficient

The transfer coefficient for the liquid phase was obtained from the literature (Jury, 2007; Ni et al., 1999; Zhang and Datta, 2006).

$$D_l^W = -10^{-6}\exp(-10+10W)\varepsilon \tag{27}$$

2.4.3. Effective diffusion coefficient of the vapour

To calculate the coefficient of vapour diffusion with the water content gradient D_v^W (see Appendix A), an expression of the effective diffusion coefficient from the literature was used (Zhang and Datta, 2006).

$$D_v^{\text{eff}} = f_c D_{cv}((1-1.11S)\varepsilon)^{4/3} \tag{28}$$

2.4.4. Gas permeability

Diffusion coefficients $D_v^{P_g}$ and $D_{CO_2}^{P_g}$ use intrinsic and relative permeability. In this model, the crumb/crust transition occurs at a temperature of 100 °C with a Heaviside function. Intrinsic permeability values are different for crumb (Jury, 2007) and crust (Vanin, 2010):

$$k_{in} = \begin{cases} 8.7710^{-11}\varepsilon^{1.34} & \text{for} \quad T < 100^{\circ}C \\ 10^{-12} & \text{for} \quad T \geqslant 100^{\circ}C \end{cases} \tag{29}$$

For relative permeability, the following relation is applied (Ni et al., 1999; Zhang and Datta, 2006):

$$k_{rg} = 1 - 1.1S \tag{30}$$

2.4.5. Pore opening

At the beginning of baking, the product is a medium with essentially closed porosity (gas bubbles are not interconnected), and the gas mass transfer is off. Mass transfer occurs in the liquid phase. As the temperature increases and carbon dioxide released, the pore volume becomes significant and interconnections appear. Transfer in the gas phase becomes more consistent. To simulate pore opening, a Heaviside function (α) centred at the pore opening temperature (T_{open}) and with a range (ΔT) (Fig. 4) is used (Vanin, 2010).

2.4.6. Thermal properties

A parallel model is used for thermal conductivity. Its value depends on the volume fractions and the intrinsic conductivities of each phase (Table 1) (Jury et al., 2007).

$$\lambda = \varepsilon_s\lambda_s + \varepsilon_l\lambda_l + \varepsilon_g\lambda_g \tag{31}$$

The equivalent heat capacity is obtained by summing the volume heat capacities of each phase.

$$\rho c_p = \rho_s^a c_{p_s} + \rho_l^a c_{p_l} + \rho_g^a c_{p_g} \tag{32}$$

2.4.7. Viscoelastic properties

The viscoelastic model requires the elastic modulus and relaxation time (Fig. 5). These parameters depend on the product structure. With a low relaxation time the product is considered as a liquid. We then found a slight increase in the relaxation time during gelatinisation. In addition, a very significant increase of the properties occurs at the onset of crusting. The relaxation time has a value of 2 s for the dough, 20 s for the crumb (Zhang et al., 2005) and 2000 s for the crust.

The elastic modulus increases during gelatinisation (Vanin et al., 2009). Accordingly, the value of the elastic modulus of the dough is 2×10^4 and increases to 3×10^5 for the crumb and crust.

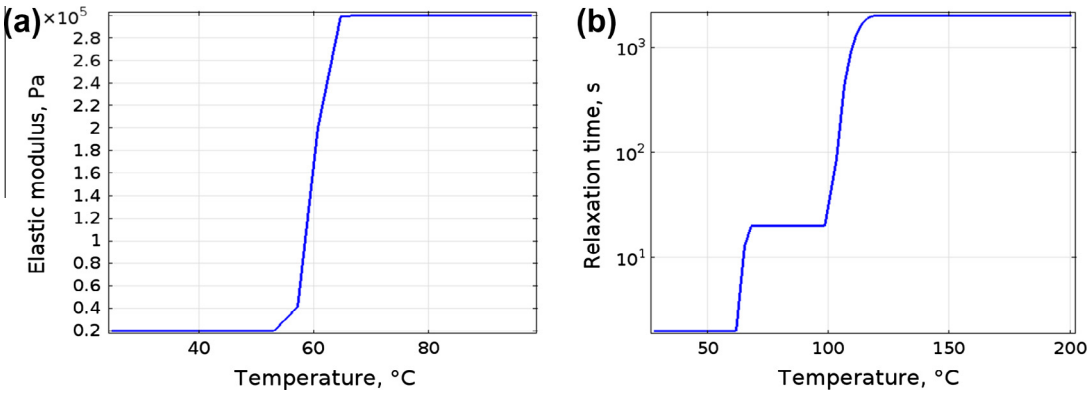

Fig. 5. Elastic modulus evolution (a) and relaxation time evolution (b) with temperature.

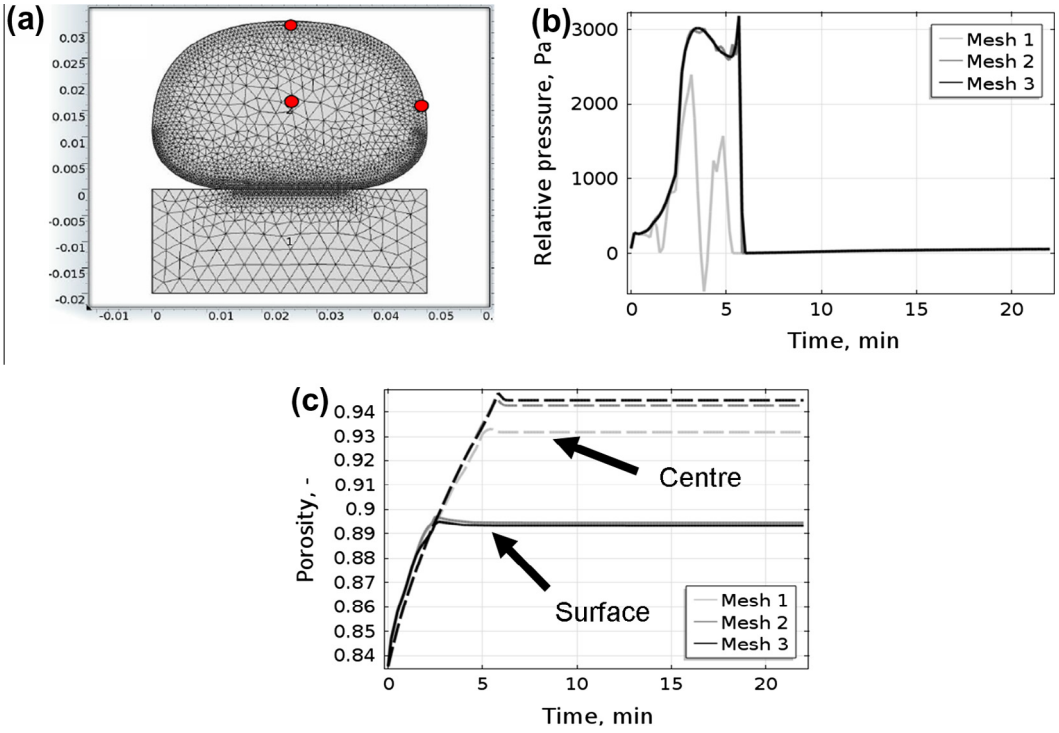

Fig. 6. Mesh chosen to be used in the model (a); mesh effect on gas pressure in the centre (b) and on porosity (c) at centre (dashed line) and surface (solid line) of the product for mesh 1 (light grey), mesh 2 (grey) and mesh 3 (black).

2.4.8. Carbon dioxide generation

Carbon dioxide generation can be explained by the anaerobic fermentation of yeast during which the latter converts the fermentable sugars into alcohol and carbon dioxide. Fermentation is temperature dependent. Carbon dioxide generation is explained as follows (Zhang and Datta, 2006):

$$K_{CO_2} = \rho_s^a R_{CO_2} \tag{33}$$

with R_{CO_2} being CO_2 generation per kilogram of dry mass. It increases to a temperature of 40 °C to reach its maximum value and then decreases rapidly to stop completely at a temperature of 55 °C, when the yeast is deactivated (Zhang et al., 2005).

$$R_{CO_2} = \begin{cases} 5.10^{-6}(T - 273.15) - 9.9810^{-5} & \text{for} \quad T \leqslant 40^{\circ}C \\ 10^{-4}\exp^{\left(-\frac{(T-Tm)}{\Delta T}\right)^2} & \text{for} \quad T \geqslant 40^{\circ}C \end{cases} \tag{34}$$

3. Preliminary numerical study

The previous model was implemented in a computer code by using the finite element method. A 2D geometry was specified (Fig. 6a) and a triangular mesh comprising 4481 elements were selected. ALE (Arbitrary Lagrangian–Eulerian formulation) formalism was used to take into account deformation. The initial characteristic dimensions of the dough were a height of 3.2 cm, a width of 5 cm and a length of 53 cm. The initial overall shape is that of a flattened ellipse. The hearth was 2 cm in height and 5 cm in width.

Table 2
Meshes characteristics.

Parameters	Mesh1	Mesh2	Mesh3
Number of element	5455	7929	18953
Maximum size element	5×10^{-3}	10^{-3}	0.5×10^{-3}

3.1. Mesh sensitivity

The simulated results presented were evaluated at the centre, on the top surface and at the sides of the product (Fig. 6a). The parameters used in the boundary conditions do not correspond to a particular baking test. External conditions (Air temperature, Infrared radiation, etc.) are left constant for this mesh sensitivity analysis.

The mesh was static for the hearth, thus a mesh created automatically by the software was sufficient. The mesh on the surface of the bread was imposed. It is therefore apparent that the mesh was actually refined in the centre of the product. Three meshes were tested (Table 2), depending on the maximum size and the number of elements.

Changes in the gas pressure with the three meshes are presented in (Fig. 6b). In this figure, the mesh has a very significant impact. We noted that the evolution of gas pressure at the centre of the product with mesh 1 was disrupted. Meshes 2 and 3 gave very similar results although mesh 3 led to less variation than mesh 2.

Evolutions of porosity (Fig. 6c) at the centre of the product were similar for all three meshes, but those of mesh 2 and 3 were closer. The change in porosity at the surface was insensitive to the mesh. This difference between meshes is due to the significant gap in the evolution of gas relative pressure with the mesh. The pressure has an impact on mechanical balance, velocity fields and thus on porosity.

Analysis of mesh sensitivity in the centre of the product was performed by varying three meshes. The mesh had little impact on most of the variables studied. The greatest difference was obtained with the evolution of gas pressure for mesh 1. This curve made it possible to exclude the first mesh. Meshes 2 and 3 exhibited small differences. However, the computation time was 4 times longer for mesh 3 than for mesh 2. Finally, mesh 2 was chosen because it provided satisfactory accuracy within a minimum calculation time.

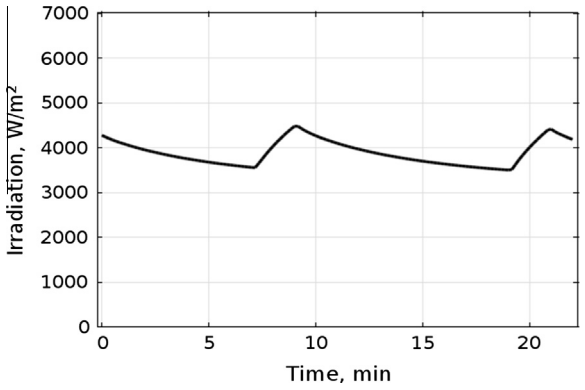

Fig. 7. Emitted infrared radiation by the oven.

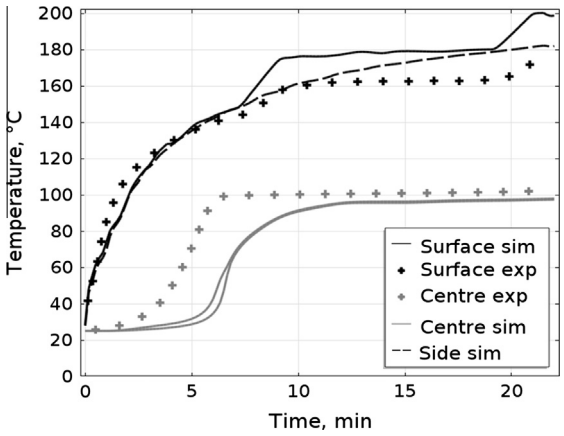

Fig. 8. Temperature evolutions for surface, centre and side of the product.

4. Results and discussion

Firstly, the simulation results are compared to the experimental measurements performed by the LIMATB laboratory (Ploteau et al., 2012). Secondly, the evolution of the model in time and space is analysed. Lastly, a parametric and sensitivity study is performed.

4.1. Experimental conditions

The dough pieces were made at a baker's referenced by the research project. This allowed us to have dough of the same quality ready to be placed in the oven. The dough pieces had an initial average mass of 335 g.

Initially the water content was around 0.82 kg kg^{-1} in the dry base and the gas fraction was 0.63 m^3 m^{-3}, deduced from the other initial conditions. Moreover, we assumed an initial gas pressure equal to atmospheric pressure and a porous matrix velocity equal to zero.

Baking was done in an instrumented electrical oven (Ploteau et al., 2012). Electrical heating elements were positioned under the upper side of the oven (vault) as well as under the hearth.

Baking took about 22 min. The temperature set points applied to the oven were 240 °C for the hearth and 230 °C for the vault.

The infrared radiation received by the product followed the variations of the vault resistor temperature (Fig. 7). The hearth temperature on the lower face was 240 °C when the baking started.

The initial air temperature was 155 °C. This low value was due to opening the door when introducing the dough. During baking, the air temperature increased to 200 °C.

Only one piece was baked by batch per test. Temperature measurements were performed in the dough by thin and flexible type K thermocouples embedded at different positions. Monitoring of mass loss and surface temperature by optical pyrometer was also performed.

4.2. Comparison of experimental and numerical results

Figs. 8 and 9 present the numerical and experimental evolutions of temperature and water content.

Firstly, we observed that the model correctly reproduced the rapid increase of surface temperature as a function of the experimental evolution (Fig. 8). The rise of the simulated surface temperature occurred after 7 min, corresponding to an increase of vault infrared radiation (Fig. 7). The difference was quite small between simulation and experiment. This difference could be introduced in the measurement uncertainty. First, it was difficult to measure surface temperature and, second, the lateral movement of the dough during baking made it difficult to perform an exact comparison between the simulation and observation. For this simulation, the heat transfer coefficient h_c at the dough-air interface obtained with Eq. (22) varied between 4 and 8 W m^{-2} K^{-1}.

The simulated temperature rose slowly in the centre of the product; it reached 100 °C after 6 min. This simulation presented a time lag of 2 min in comparison with the experimental evolution.

However, this temperature levelled out at 100 °C, observed experimentally. The plateau of 100 °C was due to the evaporation of water in the product. The difference was apparent in the temperature increase. This gap could be due to the fact that not taking into account the phenomenon of evaporation–condensation when the pores were closed. In our case this phenomenon was only taken into account when the pores were open.

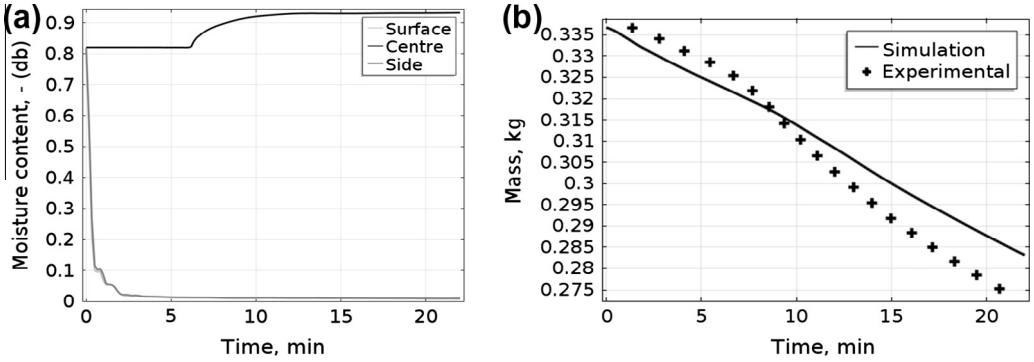

Fig. 9. Moisture content evolutions (a); Simulated (black solid line) and experimental mass evolutions (b).

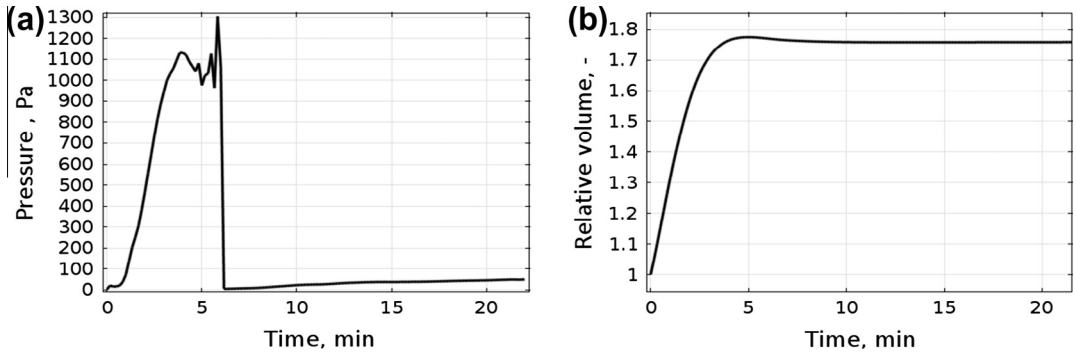

Fig. 10. Simulated gas pressure evolution in centre (a); simulated global volume (b).

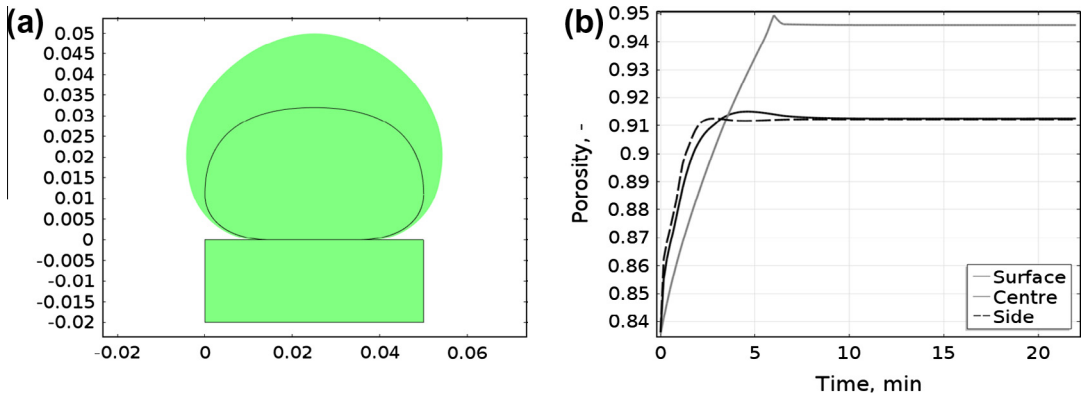

Fig. 11. Simulated global geometry (a); simulated local porosity evolution for surface, side and centre (b).

Fig. 9b shows the corresponding evolution of the mass loss obtained experimentally and by simulation. A mass loss of 50 g (15%) was observed. The average moisture content decreased from 0.82 to 0.57. The simulated evolution is in agreement with the experimental evolution. However, a difference in their kinetics can be seen. Indeed, the simulated mass loss was higher at the beginning of simulation and lower at the end.

Fig. 9a shows the simulated evolutions of the water content on the surface and at the centre. The water content on the surface decreased rapidly and fell below 0.1 kg kg^{-1} after only one minute of baking.

At the centre, the water content was constant for the first six minutes and then increased, tending towards a value of 0.9 kg kg^{-1}. Before evaporation, steam flowed to the centre of the bread. This evaporation–condensation phenomenon generated an additional heat transfer and a slight increase in water content in the centre (Thorvaldsson and Janestad, 1999; Wagner et al., 2007). The sudden increase in the water content corresponded to the pressure drop observed in Fig. 10a. This was due to the opening of the pores thus allowing gas transfer; hot steam suddenly condensed on a cold wall, leading to a local increase in water content.

4.3. Simulation of deformation/prediction of spatial–temporal evolution

Fig. 10a shows the evolution of pressure in the centre of the product. Simulated pressure evolution has never been presented in previous works on bread baking. Initially, the pressure increases, then a slight drop is observed before a short increase to a peak. Then, after 6 min, the pressure drops suddenly to remain at atmospheric pressure. This evolution is supported by other measurements (Grenier et al., 2010). The pores were closed during the pressure increase and gas transfer was locked. However, the temperature increased in the product and yeast fermentation generated bubbles of carbon dioxide. The effect of these two phenomena was an increase of the pressure in the product. The second phase of the simulation showed a sharp drop of pressure to atmospheric pressure. This drop was due to the opening of the pores which became interconnected, allowing the transfer of the gaseous phase. Then the pressure decreased in the product.

The simulated relative volume increased during the first six minutes and then stayed constant (Fig. 10b). A similar evolution was presented in a previous study (Zhang et al., 2005). The final geometry (Fig. 11a) was very similar to what was observed experimentally, with an average final height of 5 cm. The simulation of the overall deformation was satisfactory.

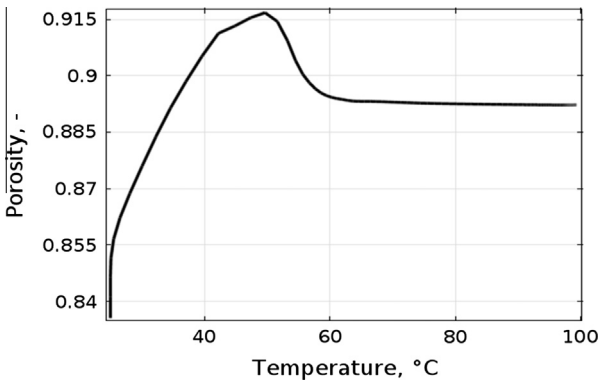

Fig. 12. Simulated porosity evolution in the centre compared with temperature.

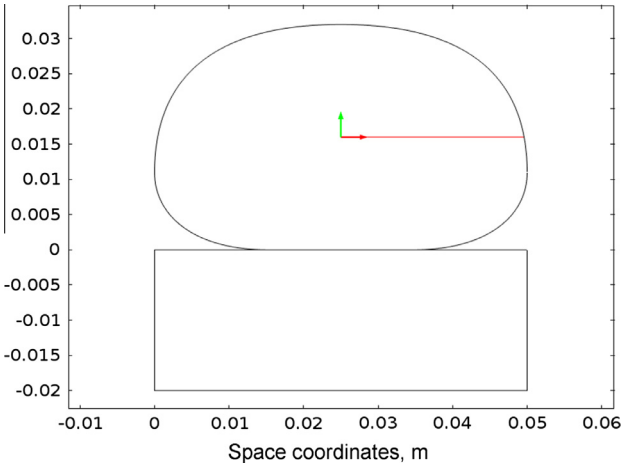

Fig. 13. Section used to evaluate spatial evolution.

The simulation of porosity (Fig. 11b), presented for the first time, was directly dependent on the velocity field calculated by the mechanical model. We noted that the end of the increase of porosity in the centre coincided with the increase in pressure and thus with pore opening at 55 °C (Fig. 12). This highlighted the link between pressure, porosity and deformation. In this article we consider porosity as the fraction of void volume (liquid + gas) and total volume. The high porosity values stem from this definition. As explained before, the gas fraction, known as "porosity" in the bakery community, is initially equal to 0.63.

The mechanical model used does not describe all the crusting phenomena (scarification, compression, etc.). Simulated crust porosity increases due to the material pushing beneath the surface. As the surface has not yet solidified, displacement occurs in the solid matrix and porosity increases.

Geometric evaluation was performed to determine the evolution of variables as a function of space at different simulation times (Fig. 13).

After one minute, surface water content decreased sharply while the rest of the product stayed at the initial value. We noted that the water content increased by 0.0525 m at the abscissa (Fig. 14a). Then, the increase in water content progressed towards the centre of the product to a maximum value of 0.9 kg kg^{-1}. This increase was also simulated in a previous study (Thorvaldsson and Janestad, 1999). At the same time, the water content at the surface continued to decrease.

By zooming on the area near the surface in Fig. 14b, it is possible to observe the spatial evolution of the water content more precisely. We noted that the transition from high water content to low water content occurred within a narrow zone, resulting in a high gradient. The product changed from a wet material, also called "dough or crumb," to a dry one near the surface which can be identified clearly at the crust.

This transition zone corresponds to the evaporation front (Zanoni et al., 1993). During the simulation, the evaporation front moved towards the interior of the geometry. This advance corresponded to an increase in the thickness of the crust during baking, in this case 5 mm after 15 min simulation.

On examining the spatial evolution of the temperature (Fig. 14c), it can be seen that, initially, the temperature increases rapidly near the surface while it increases more slowly at the centre. This observation is logical because there is no internal heat source in the product. The flow of heat by conduction and condensation is directed to the centre of the product. Here, the

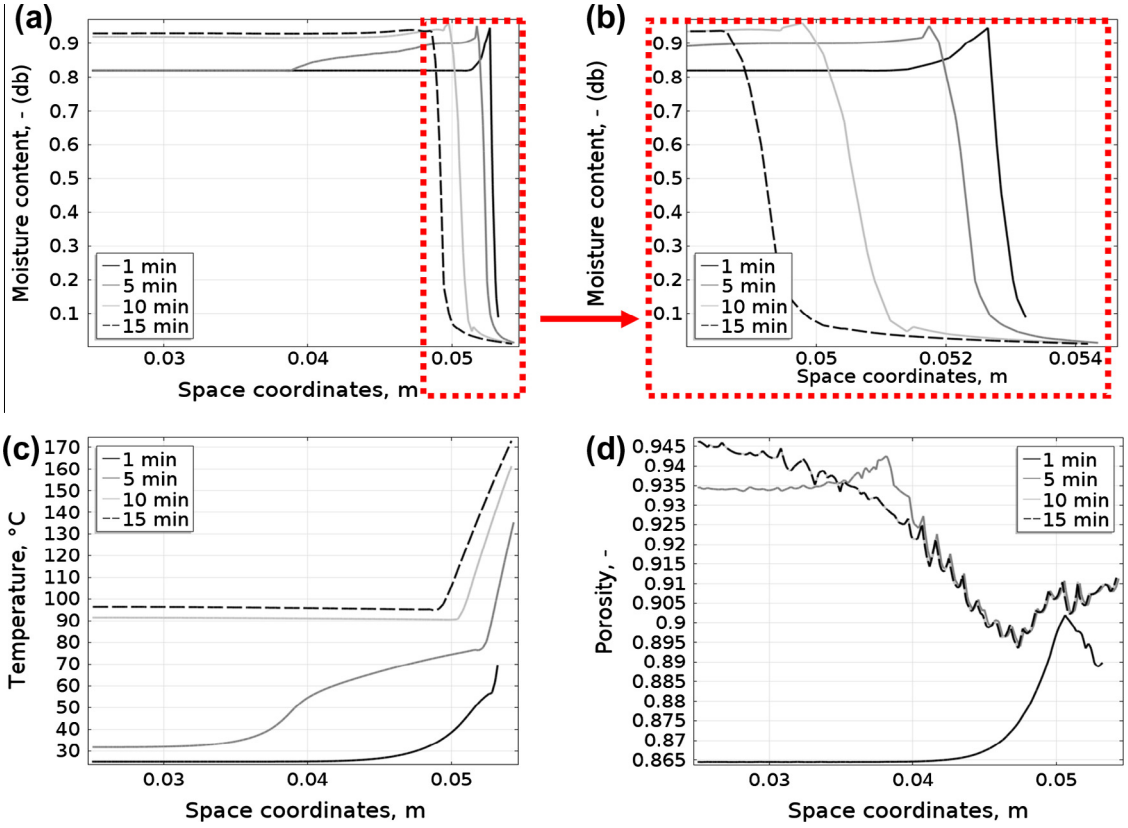

Fig. 14. Spatial evolution of moisture content (a); zoom of the dotted area (b); spatial evolution of temperature (c) and porosity (d) at 1 min (black solid line), 5 min (grey solid line), 10 min (light grey solid line) and 15 min (black dashed line).

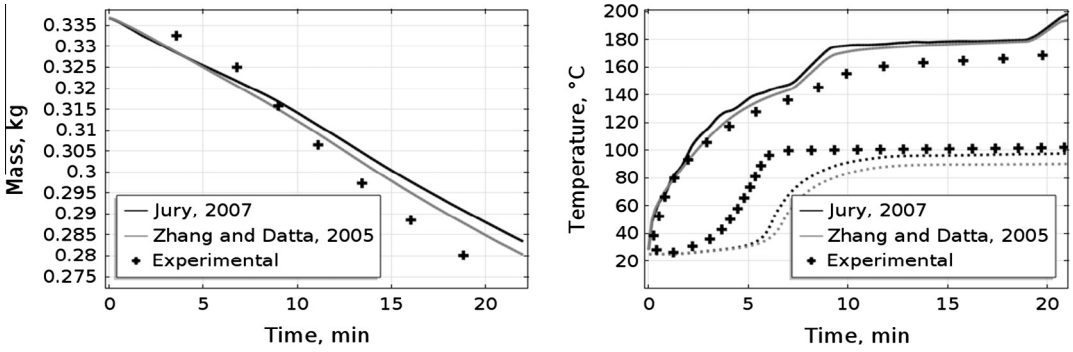

Fig. 15. Evolution of mass and temperature with water activity.

temperature increases to 100 °C. Near the surface, the temperature rises sharply due to the passage in the dry zone where the water content is low.

It is interesting to observe the evolution of the porosity as a function of space at different times (Fig. 14d). Initially, the increase in porosity first occurs at the exterior of the product and moves towards the centre at a higher amplitude. However, there is a zone of lower porosity between abscissas 0.045 m and 0.05 m. This area has already been observed (Vanin et al., 2009). The crumb, located near the crust, is compressed. This results in a decrease of porosity in this area.

This part shows the interest of using a multiphase model which is capable of calculating the gas pressure. It was this gas pressure that was implemented in the mechanical model to calculate the evolution of local porosity.

4.4. Parametric study

4.4.1. Water activity

Water activity is a significant parameter for a baking model. Two models of water activity were used in this study and compared: a model corresponding to measurements (Jury, 2007) and a fitted model (Zhang and Datta, 2006). In fact, the numerical bread baking simulation model formulated using the fitted model failed to identify the weight loss of the experimental model of water activity based on the experimental points of Lind and Rask (1991). This led them to change parameters A and B of Oswin's model to find the correct weight loss. Mass and temperature are compared for the two models in Fig. 15.

For the overall mass and volume, no major difference was observed between the two simulations. For the temperature at the centre, the evolution observed with Zhang's and Datta's water activity model (2006) was lower than the temperature evolution obtained with Jury's water activity model (2007). This difference is due to lower activity (Fig. 3). The mass flow of evaporation is lower, the water content decreases more slowly, with the effect of maintaining high thermal conductivity.

The evolution of activity had an impact on the vapour diffusion coefficient. In fact, the water vapour diffusion coefficient depended on the derivative of the activity in relation to the temperature and water content. With the model of Zhang and Datta (2006), the derivative of the activity in relation to the water content was lower

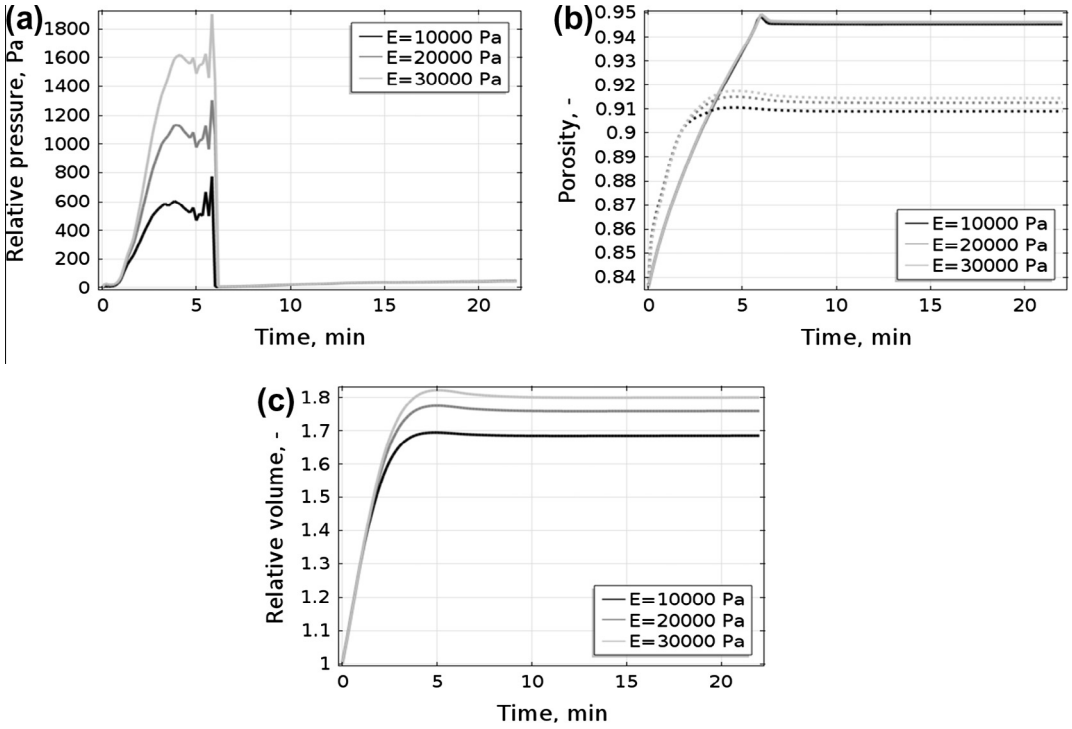

Fig. 16. Evolution of relative pressure (a), porosity (b) and deformation (c) with evolution of three dough elastic modulus values (1×10^4 black line, 2×10^4 grey line and 3×10^4 light grey line).

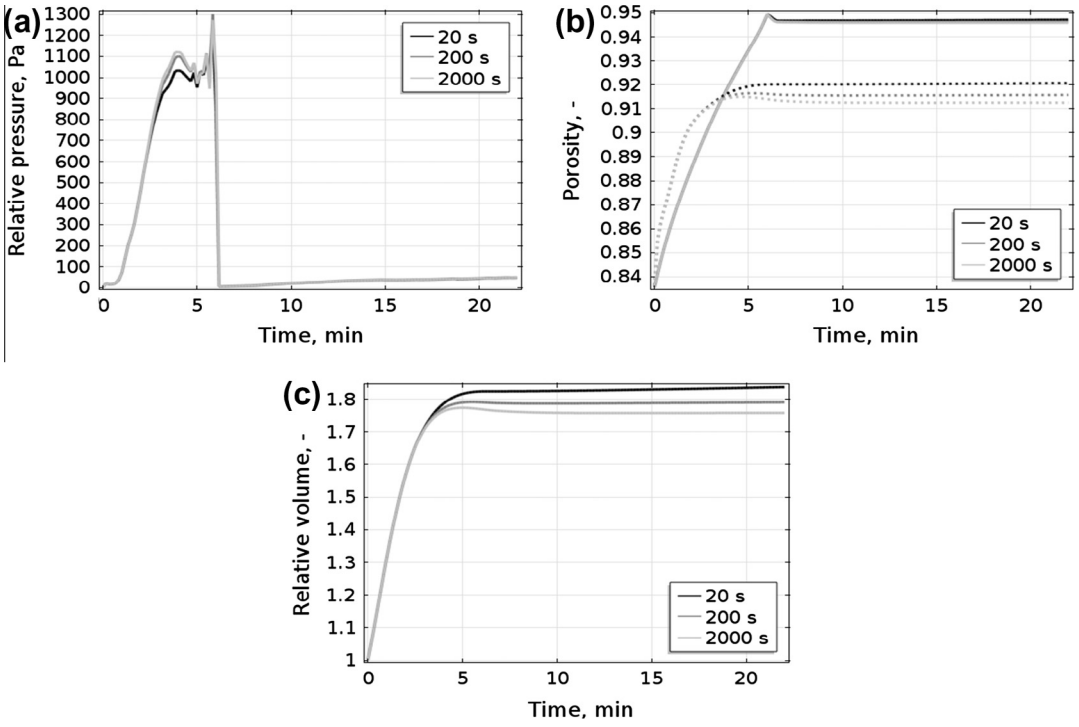

Fig. 17. Evolution of relative pressure (a), porosity (b) and deformation (c) with evolution of three crust relaxation time values (20s black line, 200s grey line and 2000s light grey line).

and the diffusion coefficient became smaller. Therefore, the diffusion of the steam in the product was lower and the water content condensed, at least in the product, slowing down the temperature increase at the centre.

The water activity finally used by the model was experimental. Indeed, the changes observed in this model match the experimental evolution better (surface water content and temperature at the centre), whereas the other changes are nonsignificant.

4.4.2. Dough elastic modulus

The scientific literature abounds with measurements of elastic modulus. The value chosen was based on the measurements of Rouillé et al. (2010) and the evolutions of mechanical properties

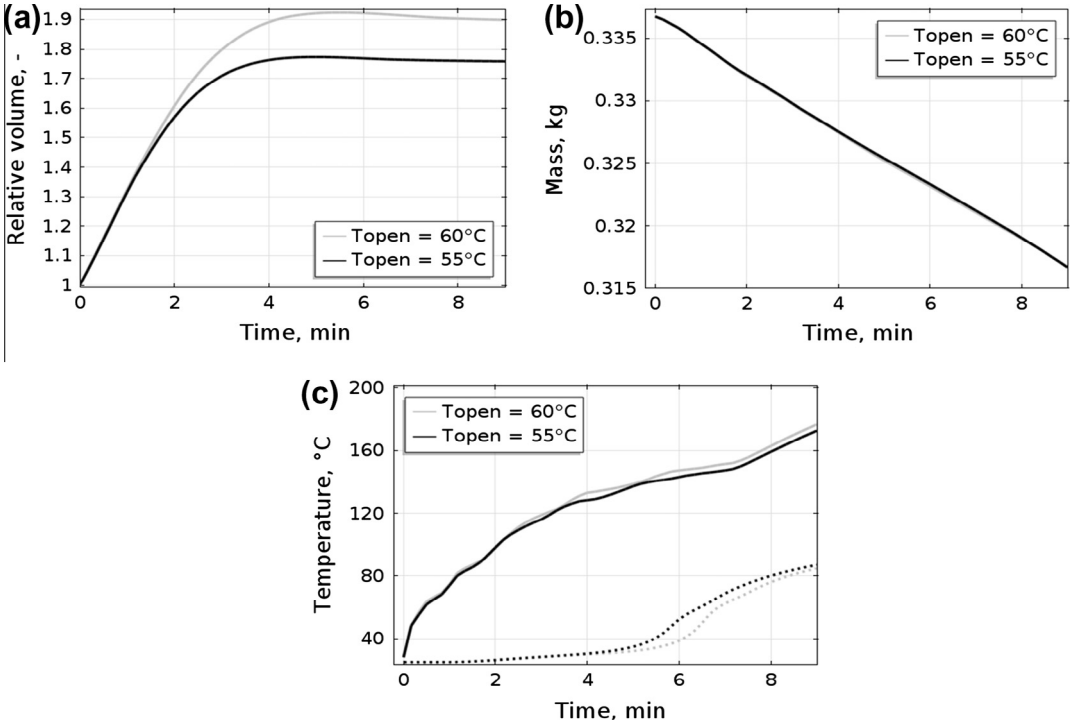

Fig. 18. Evolutions of deformation (a), mass (b) and temperature (c) with evolution of two pore opening temperature values (55 °C black line, 60 °C grey line).

had a significant impact on the evolution of deformation (local and global) and pressure. Here, the impact of the elastic modulus of the dough on deformation was studied by introducing three values (Fig. 16): 10,000, 20,000 and 30,000 Pa. The values selected were chosen to be close to reality. An action on the elastic modulus did not affect the rate of change of the relative volume. We noted only that an increase in this modulus resulted in a stronger variation. There was also significant sensitivity to this pressure. Consequently, the higher the modulus, the higher the pressure.

4.4.3. Crust relaxation time

Zhang et al., 2005 proposed a relaxation time value for dough and crumb. A value higher than that of the crumb value was assumed to simulate solid a material like crust. This is why the sensitivity study was performed with higher values. Unlike the variation of the elastic modulus of the dough, increasing crust relaxation time tended to decrease deformation (Fig. 17). We also noted the low impact of the evolution of relaxation time on the evolution of the pressure at the centre of the product.

4.4.4. Pore opening temperature

In this study, the pore opening temperature was imposed at a value of 60 °C (Fig. 18). The results were compared to a reference simulation at 55 °C. The fact of shifting the temperature of the pore opening to 60 °C resulted in greater deformation. Indeed, this stopped gas transfer for temperatures below T_{open}. Stopping the transfer of gas increased the pressure in the product and greater deformation was observed. If the temperature of the pore opening was higher, gas transfer occurred later and pressure increased over time, resulting in a larger volume.

5. Conclusions

A multiphase model for simulating heat and mass transfer in a deformable medium was presented. It consisted of several partial differential equations having the following state variables: water content (dry base), temperature, gas pressure, gas fraction and deformation.

The boundary conditions were developed for a batch type oven with natural convection and a hearth. The particularity of this model was that it took into account the exchange between the bread and the hearth by introducing a thermal contact resistance at the interface and modelling the heat transfer in the hearth.

The advantage of using a multiphase model was shown, as it allows simulating other phenomena such as the evolution of pressure and local porosity.

The sensitivity study showed:

- A slight difference between the two activity models. In conclusion, a model based on experimental activity was chosen.
- The variations of dough elastic modulus highlighted a considerable effect on volume and pressure. A shift of 5 degrees for the pore opening temperature had a significant impact on the simulated deformation.
- A high value of crust relaxation time was used.
- The open temperature was an important parameter for obtaining the experimental evolution.

The comparison between the simulated and experimental results showed that the model gives the evolutions in temperature, mass and deformation corresponding to classical baking. The differences were due to measurement uncertainties but also to phenomenon not taken into account in the numerical model. Despite of the complexity of the model, different aspects can be improved:

- The temperature at the centre of the product could be improved by taking into account the evaporation condensation phenomenon at closed porosity.
- The addition of a conservation equation of dry air entering the product when carbon dioxide escapes.
- The mechanical behaviour of crumb and crust must be better described by adding gravity and shrinkage.

These developments require complete experimental data (measurement of properties, carbon dioxide production).

In reality, steam is injected into the oven at the beginning of the baking process. This injection helps to add colour to the product and should be introduced in the model to achieve the final goal of simulating the entire process.

Acknowledgements

This work was carried out with financial support from the French National Research Agency (ANR-"BRAISE") in the framework of the "ALIA" program, and the VALORIAL cluster. The authors wish to thank Bongard, their industrial partner.

Appendix A

$$D_v^W = -D_v^{\text{eff}} \frac{M_v M_{CO_2}}{M_g \text{RT}} \frac{\partial P_v}{\partial W} \tag{A.1}$$

$$D_v^T = -D_v^{\text{eff}} \frac{M_v M_{CO_2}}{M_g \text{RT}} \frac{\partial P_v}{\partial T} \tag{A.2}$$

$$D_v^{P_g} = D_v^{\text{eff}} \frac{M_v M_{CO_2}}{M_g \text{RT}} \frac{P_v}{P_g} - \rho_v^i \frac{k_{in} k_{rg}}{\mu_g} \tag{A.3}$$

$$D_{CO_2}^W = D_v^{\text{eff}} \frac{M_v M_{CO_2}}{M_g \text{RT}} \frac{\partial P_v}{\partial W} = -D_v^W \tag{A.4}$$

$$D_{CO_2}^T = D_v^{\text{eff}} \frac{M_v M_{CO_2}}{M_g \text{RT}} \frac{\partial P_v}{\partial T} = -D_v^T \tag{A.5}$$

$$D_{CO_2}^{P_g} = -D_v^{\text{eff}} \frac{M_v M_{CO_2}}{M_g \text{RT}} \frac{P_v}{P_g} - \rho_{CO_2}^i \frac{k_{in} k_{rg}}{\mu_g} \tag{A.6}$$

$$\gamma_1 = \frac{\varepsilon(1-S) M_{CO_2}}{\text{RT}} \left[\frac{(P_v - P_g)}{T} - \frac{\partial P_v}{\partial T} \right] \tag{A.7}$$

$$\gamma_2 = -\frac{\varepsilon M_{CO_2}(1-S)}{\text{RT}} \left[\frac{\partial P_v}{\partial W} + \frac{\rho_s^a}{\varepsilon \rho_l^i} \frac{(P_g - P_v)}{(1-S)} \right] \tag{A.8}$$

$$\gamma_3 = \frac{\varepsilon(1-S) M_{CO_2}}{\text{RT}} \tag{A.9}$$

$$\gamma_4 = \frac{P_{CO_2} M_{CO_2}}{\text{RT}} \tag{A.10}$$

Appendix B. Expression of ζ_1 and ζ_2 coefficients

$$\frac{\partial \rho_l^a}{\partial t} = \frac{\partial \rho_s^a W}{\partial t} = \rho_s^a \frac{\partial W}{\partial t} + W \frac{\partial \rho_s^a}{\partial t} \tag{B.1}$$

$$\frac{\partial \rho_s^a}{\partial t} = \frac{\partial \left(\rho_s^i (1-\varepsilon) \right)}{\partial t} = \rho_s^i \frac{\partial (1-\varepsilon)}{\partial t} = -\rho_s^i \frac{\partial \varepsilon}{\partial t} \tag{B.2}$$

With porosity, the sum of gas and liquid volume fraction

$$\varepsilon = \varepsilon_l + \varepsilon_g \tag{B.3}$$

$$\frac{\partial \varepsilon}{\partial t} = \frac{\partial \varepsilon_l}{\partial t} + \frac{\partial \varepsilon_g}{\partial t} \tag{B.4}$$

$$\frac{\partial \rho_l^a}{\partial t} = \frac{\partial \rho_s^a W}{\partial t} = \rho_s^a \frac{\partial W}{\partial t} + W\left(-\rho_s^i \frac{\partial \varepsilon}{\partial t}\right) \tag{B.5}$$

$$\begin{aligned}\frac{\partial \rho_l^a}{\partial t} &= \rho_s^a \frac{\partial W}{\partial t} - W\rho_s^i\left(\frac{\partial \varepsilon_l}{\partial t} + \frac{\partial \varepsilon_g}{\partial t}\right) \\ &= \rho_s^a \frac{\partial W}{\partial t} - W\rho_s^i \frac{\partial \varepsilon_l}{\partial t} - W\rho_s^i \frac{\partial \varepsilon_g}{\partial t}\end{aligned} \tag{B.6}$$

$$\frac{\partial \varepsilon_l}{\partial t} = \frac{\partial\left(\rho_l^a/\rho_l^i\right)}{\partial t} = \frac{1}{\rho_l^i}\frac{\partial \rho_l^a}{\partial t} = \frac{1}{\rho_l^i}\frac{\partial\left(\rho_s^a W\right)}{\partial t} \tag{B.7}$$

$$\frac{\partial \rho_l^a}{\partial t} = \frac{\rho_s^a \rho_l^i}{\left(\rho_l^i + W\rho_s^i\right)}\frac{\partial W}{\partial t} - \frac{W\rho_s^i \rho_l^i}{\left(\rho_l^i + W\rho_s^i\right)}\frac{\partial \varepsilon_g}{\partial t} \tag{B.8}$$

With final expression:

$$\frac{\partial \rho_l^a}{\partial t} = \zeta_1 \frac{\partial W}{\partial t} - \zeta_2 \frac{\partial \varepsilon_g}{\partial t} \tag{B.9}$$

$$\zeta_1 = \frac{\rho_s^a \rho_l^i}{\left(\rho_l^i + W\rho_s^i\right)} \tag{B.10}$$

$$\zeta_2 = \frac{W\rho_s^i \rho_l^i}{\left(\rho_l^i + W\rho_s^i\right)} \tag{B.11}$$

Appendix C. Expressions of β_1, β_2 and β_3 coefficients

$$\begin{aligned}\frac{\partial \rho_v^a}{\partial t} &= \frac{\partial\left(\varepsilon_g \frac{P_v M_v}{RT}\right)}{\partial t} = \frac{M_v}{R}\frac{\partial\left(\varepsilon_g \frac{P_v}{T}\right)}{\partial t} = \frac{M_v}{R}\left[\frac{1}{T}\frac{\partial\left(\varepsilon_g P_v\right)}{\partial t} - \frac{1}{T^2}\varepsilon_g P_v \frac{\partial T}{\partial t}\right] \\ &= \frac{M_v}{R}\left[\frac{1}{T}\left(\frac{\varepsilon_g \partial P_v}{\partial t} + \frac{P_v \partial \varepsilon_g}{\partial t}\right) - \frac{1}{T^2}\varepsilon_g P_v \frac{\partial T}{\partial t}\right]\end{aligned} \tag{C.1}$$

$$\frac{\partial \rho_v^a}{\partial t} = \frac{M_v}{R}\left[\frac{1}{T}\frac{\varepsilon_g \partial P_v}{\partial t} - \frac{1}{T^2}\varepsilon_g P_v \frac{\partial T}{\partial t} + \frac{1}{T}\frac{P_v \partial \varepsilon_g}{\partial t}\right] \tag{C.2}$$

$$\frac{\partial \rho_v^a}{\partial t} = \varepsilon_g \frac{M_v}{RT}\left(\frac{\partial P_v}{\partial T} - \frac{P_v}{T}\right)\frac{\partial T}{\partial t} + \varepsilon_g \frac{M_v}{RT}\frac{\partial P_v}{\partial W}\frac{\partial W}{\partial t} + \frac{M_v P_v}{RT}\frac{\partial \varepsilon_g}{\partial t} \tag{C.3}$$

With final expression:

$$\frac{\partial \rho_v^a}{\partial t} = \beta_1 \frac{\partial T}{\partial t} + \beta_2 \frac{\partial W}{\partial t} + \beta_3 \frac{\partial \varepsilon_g}{\partial t} \tag{C.4}$$

$$\beta_1 = \varepsilon_g \frac{M_v}{RT}\left(\frac{\partial P_v}{\partial T} - \frac{P_v}{T}\right) \tag{C.5}$$

$$\beta_2 = \varepsilon_g \frac{M_v}{RT}\frac{\partial P_v}{\partial W} \tag{C.6}$$

$$\beta_3 = \frac{M_v P_v}{RT} \tag{C.7}$$

References

Bellido, G.G., Scanlon, M.G., Sapirstein, H.D., Page, J.H., 2008. Use of a pressuremeter to measure the kinetics of carbon dioxide evolution in chemically leavened wheat flour dough. J. Agric. Food Chem. 56, 9855–9861.

Bellido, G.G., Scanlon, M.G., Page, J.H., 2009. Measurement of dough specific volume in chemically leavened dough systems. J. Cereal Sci. 49, 212–218.

Bird, R.B., Stewart, W.E., Lightfoot, E.N., 2002. Transport Phenomena. Wiley.

Bishop, A.W., 1960. The Principle of Effective Stress. Norges Geotekniske Inst..

Cáceres Salazar, G., 2006. Modeling of drying for a saturated deformable porous media: taking into account the liquid pressure (Thesis). Ecole Nationale Supérieure d'Arts et Métiers. Bordeaux.

Chemkhi, S., Zagrouba, F., 2008. Development of a Darcy-flow model applied to simulate the drying of shrinking media. Braz. J. Chem. Eng. 25.

Chiotellis, E., Campbell, G.M., 2003a. Proving of bread dough I: modelling the evolution of the bubble size distribution. Food Bioprod. Process. 81, 194–206.

Chiotellis, E., Campbell, G.M., 2003b. Proving of bread dough II: Measurement of gas production and retention. Food Bioprod. Process. 81, 207–216.

Dhall, A., Datta, A.K., 2011. Transport in deformable food materials: a poromechanics approach. Chem. Eng. Sci. 66, 6482–6497.

Fan, J., Mitchell, J.R., Blanshard, J.M.V., 1999. A model for the oven rise of dough during baking. J. Food Eng. 41, 69–77.

Grenier, D., Le Ray, D., Lucas, T., 2010. Combining local pressure and temperature measurements during bread baking: insights into crust properties and alveolar structure of crumb. J. Cereal Sci. 52 (1), 1–8. http://dx.doi.org/10.1016/j.jcs.2009.09.009.

Hussein, M., Becker, T., 2010. An innovative micro-modelling of simultaneous heat and moisture transfer during bread baking using the Lattice Boltzmann method. Food Biophys. 5, 161–176.

Incropera, F.P., DeWitt, D.P., 2002. Fundamentals of Heat and Mass Transfer, fifth ed. John Wiley and Sons.

Jury, V., 2007. Coupled heat and mass transfer in a cellular matrix: application to thawing–baking of partially baked bread. (Thesis). ENITIAA, Nantes.

Jury, V., Monteau, J.-Y., Comiti, J., Le-Bail, A., 2007. Determination and prediction of thermal conductivity of frozen part baked bread during thawing and baking. Food Res. Int. 40, 874–882.

Lind, I., Rask, C., 1991. Sorption isotherms of mixed minced meat, dough, and bread crust. J. Food Eng. 14, 303–315.

Lostie, M., Peczalski, R., Andrieu, J., Laurent, M., 2002. Study of sponge cake batter baking process. II – Modeling and parameter estimation. J. Food Eng. 55, 349–357.

Lostie, M., Peczalski, R., Andrieu, J., 2004. Lumped model for sponge cake baking during the "crust and crumb" period. J. Food Eng. 65, 281–286.

Mondal, A., Datta, A.K., 2008. Bread baking – a review. J. Food Eng. 86, 465–474.

Ni, H., Datta, A.K., Torrance, K.E., 1999. Moisture transport in intensive microwave heating of biomaterials: a multiphase porous media model. Int. J. Heat Mass Transf. 42, 1501–1512.

Ousegui, A., Moresoli, C., Dostie, M., Marcos, B., 2010. Porous multiphase approach for baking process – explicit formulation of evaporation rate. J. Food Eng. 3, 535–544.

Ploteau, J.P., Nicolas, V., Glouannec, P., 2012. Numerical and experimental characterization of a batch bread baking oven. Appl. Therm. Eng. 48, 289–295.

Purlis, E., Salvadori, V.O., 2009a. Bread baking as a moving boundary problem. Part 1: Mathematical modelling. J. Food Eng. 91, 428–433.

Purlis, E., Salvadori, V.O., 2009b. Bread baking as a moving boundary problem. Part 2: Model validation and numerical simulation. J. Food Eng. 91, 434–442.

Purlis, E., Salvadori, V.O., 2010. A moving boundary problem in a food material undergoing volume change – simulation of bread baking. Food Res. Int. 43, 949–958.

Rouillé, J., Chiron, H., Colonna, P., Della Valle, G., Lourdin, D., 2010. Dough/crumb transition during French bread baking. J. Cereal Sci. 52, 161–169.

Salagnac, P., Glouannec, P., Lecharpentier, D., 2004. Numerical modeling of heat and mass transfer in porous medium during combined hot air, infrared and microwaves drying. Int. J. Heat Mass Transf. 47, 4479–4489.

Stampfli, L., Nersten, B., 1995. Emulsifiers in bread making. Food Chem. 52, 353–360.

Thorvaldsson, K., Janestad, H., 1999. A model for simultaneous heat, water and vapour diffusion. J. Food Eng. 40, 167–172.

Tong, C.H., Lund, D.B., 1993. Microwave heating of baked dough products with simultaneous heat and moisture transfer. J. Food Eng. 19, 319–339.

Vanin, F.M., 2010. Crust formation during baking: an experimental and modelling approach. (Thesis). Institut des Sciences et Industries du vivant et de l'Environnement (AgroParisTech).

Vanin, F.M., Lucas, T., Trystram, G., 2009. Crust formation and its role during bread baking. Trends Food Sci. Technol. 20, 333–343.

Wagner, M.J., Lucas, T., Le Ray, D., Trystram, G., 2007. Water transport in bread during baking. J. Food Eng. 78, 1167–1173.

Zanoni, B., Peri, C., Pierucci, S., 1993. A study of the bread-baking process. I: A phenomenological model. J. Food Eng. 19, 389–398.

Zanoni, B., Pierucci, S., Peri, C., 1994. Study of the bread baking process–II. Mathematical modelling. J. Food Eng. 23, 321–336.

Zhang, J., Datta, A.K., 2006. Mathematical modeling of bread baking process. J. Food Eng. 75, 78–89.

Zhang, J., Datta, A.K., Mukherjee, S., 2005. Transport processes and large deformation during baking of bread. AIChE J. 51, 2569–2580.